Thin-Film-Mediated Deformation of Droplet during Cryopreservation

Jochem G. Meijer[1,*] Pallav Kant[1,†] Duco van Buuren,[1] and Detlef Lohse[1,2,‡]

[1]*Physics of Fluids Group, Max Planck Center Twente for Complex Fluid Dynamics,*
Department of Science and Technology, Mesa+ Institute
and J. M. Burgers Center for Fluid Dynamics, University of Twente,
P.O. Box 217, 7500 AE Enschede, The Netherlands
[2]*Max Planck Institute for Dynamics and Self-Organization, Am Faberg 17, 37077 Gttingen, Germany*

Freezing of dispersions is omnipresent in science and technology. While the passing of a freezing front over a solid particle is reasonably understood, this is not so for soft particles. Here, using an oil-in-water emulsion as a model system, we show that when engulfed into a growing ice front, a soft particle severely deforms. This deformation strongly depends on the engulfment velocity V, even forming pointy-tip shapes for low values of V. We find such singular deformations are mediated by interfacial flows in *nanometric* thin liquid films separating the nonsolidifying dispersed droplets and the solidifying bulk. We model the fluid flow in these intervening thin films using a lubrication approximation and then relate it to the deformation sustained by the dispersed droplet.

Solidification of a liquid seeded with insoluble particles is pertinent to numerous natural and industrial processes, including metal processing [1–4], cryopreservation of biological cells and tissues [5–7], food engineering (ice cream making) [8–10], and swelling of wet ground (frost heaving) in colder regions [11–13]. The key feature of the solidification in such complex systems is the interaction between dispersed particles and a growing crystal (or polycrystalline structure; for short, we will use "crystal" in this Letter). When a growing crystal encounters a foreign particle suspended in a melt, the moving solidification front (a solid-liquid interface) either deforms around the particle to trap it within the crystal or rejects it [14–16]. The type of behavior that prevails at a given solidification velocity, therefore, has important implications for the microstructure of the newly formed solidified material. The interaction between a dispersed particle and the moving solidification front is dictated by an interplay among van der Waals interactions, thermal conductivity differences between the particle and the melt, solid-liquid interfacial energy, and the density change caused by the liquid-solid phase transition [17–25]. In case of a droplet or a bubble suspended in the melt, this local dynamics is amplified by thermocapillary effects [15,26,27].

In this Letter, we report a surprising and highly interesting solidification behavior that emerges when a liquid seeded with droplets of another immiscible liquid (emulsion) solidifies. We demonstrate that the dispersed nonsolidifying droplet sustains varying degree of deformations, which strongly depend on the engulfment velocity V, remarkably even forming a pointy tearlike shape for extremely slow engulfment. We find such deformation to be mediated by interfacial flows in the intervening thin liquid films that separate the dispersed droplet and the solidifying bulk. These findings are extremely relevant for exerting better control over cryopreservation procedures of food emulsions and bio-specimens, where mechanical deformations of the dispersed medium dictate the freeze-thaw stability of the solidified material. More specifically, our findings quantitatively explain why—perhaps counterintuitively—faster freezing is less intrusive for the shape of the frozen soft structures.

We investigate the interaction between an advancing water-ice freezing front and silicone oil droplets in a horizontal Hele-Shaw cell of thickness 200 μm, filled with an oil-in-water emulsion. The emulsion is prepared using a microfluidic setup, as explained in Ref. [28]. To ensure the stability of the emulsion, a surfactant TWEEN80 (Sigma-Aldrich, Germany) is added to the water (0.5 vol % initially). Since surfactants are known to affect the freezing of complex liquids [16,29,30], the prepared emulsion sample is further diluted to achieve low surfactant concentration (0.01 vol%). As a consequence, any such solutal effects are irrelevant for our experiments. In each experiment, the Hele-Shaw cell is translated at constant velocity V through a fixed temperature gradient $G = \nabla T$ using a linear actuator (Physik Instrumente, M-230.25) such that the position of the moving solidification front remains fixed in the lab frame of reference. The temperature gradient $G \sim 10 \text{ K cm}^{-1}$ is applied over the entire length of the Hele-Shaw cell by placing it over a copper block with cold and warm ends, maintained at fixed temperatures using Peltier elements. Here, we report experiments for different advancing velocities that ensure
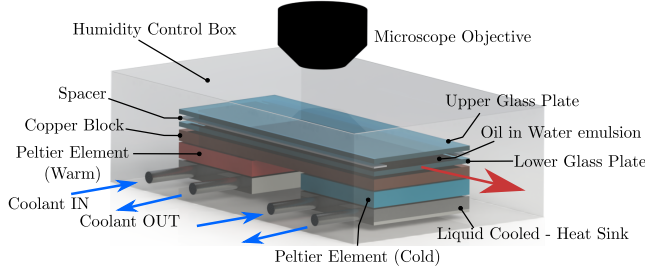
FIG. 1. Schematic of the experimental setup. The red arrow indicates the direction of sliding of the Hele-Shaw cell over the copper block.

engulfment [24], which were achieved by changing the thermal gradient G; for more details we refer to the Supplemental Material [31]. The engulfment process of a droplet into growing ice is recorded in top view through a camera connected to a long working distance lens (Thorlabs, MVL12X12Z), and diffused back lighting. A schematic of the experimental setup is given in Fig. 1.

The sequence of images in Fig. 2 depicts typical deformations experienced by an oil droplet of radius $R \sim 90 \ \mu m$ while being engulfed in the solidifying bulk at a constant advancing velocity V (Supplemental Movie 1). During the engulfment process, the initially planar solidification interface, approaching the droplet at a constant velocity $V \sim 0.4 \ \mu m \, s^{-1}$, deforms locally to envelop the droplet. Interestingly, this causes the droplet to squeeze laterally and stretch longitudinally at the opposite free end. This deformation of the droplet is characterized by its instantaneous aspect ratio $\Gamma(t)$, defined as the ratio of maximum longitudinal and lateral dimensions. Deformation curves shown in Fig. 3(a) highlight scenarios when a droplet is engulfed into the solidifying bulk at different engulfment velocities. In all cases, the droplet starts to deform soon after the advancing solidification front makes contact with it at $t = t_0$, and steadily stretches to its equilibrium state characterized by aspect ratio Γ_∞ when completely engulfed. Remarkably, the extent of deformation sustained by the droplet shows a crucial dependence on the advancing velocity V of the solidification front and

hence on the applied temperature gradient G. Note that a simple scaling analysis that balances the rate of heat released during solidification ($\rho \mathcal{L} V$) with its conduction through the solidified bulk ($k_s G$) dictates $V \propto G$; here, ρ and $\mathcal{L}$ are the density and the latent heat of water, k_s is the thermal conductivity of ice. At lower engulfment velocities (low G), the droplet severely stretches longitudinally into a tearlike shape, whereas, at increased engulfment velocities (high G), the droplet retains its initial spherical shape. The decreasing trend of Γ_∞ with advancing velocity V of the solidification front is shown in Fig. 3(b) for two kinematic viscosities. The latter does not seem to significantly influence the observed behavior. It is important to highlight that during an experiment, which typically lasts ~ 4 h, the deformed droplet retains its pointy shape once encapsulated into the solidified bulk.

The physical mechanism that causes the deformation of a droplet during the encapsulation process is intimately connected to the phenomenon known as interfacial premelting [32–34]. It is known that at constant pressure, the melting of a bulk solid occurs at a fixed temperature T_m. However, as the solid-liquid interface deforms around the droplet, the local melting temperature of the surrounding solidifying phase reduces below T_m by an amount proportional to the local curvature of the particle $(1/R)$, and the surface energy of the solidification front σ_{sl}. This reduction in local melting temperature at the expense of interfacial energy is referred to as the Gibbs-Thomson effect [35]. Moreover, when the distance between the advancing solidification front and the droplet reduces to extremely low values, less than a micrometer, van der Waals interactions become significant, giving rise to a disjoining pressure Π [36], which causes a further local reduction of the melting temperature. Therefore, the overall reduction in the local melting temperature due to the geometrical shape of the droplet and intermolecular interactions is given by [37]

$$\Delta T_m = T_m \left[\frac{\sigma_{sl}}{\rho_s \mathcal{L} R} + \left(\frac{\lambda}{H} \right)^\eta \right], \qquad (1)$$

where ρ_s is the density of the solid, $\mathcal{L}$ is the latent heat, H is the distance between the droplet interface and the front, λ is
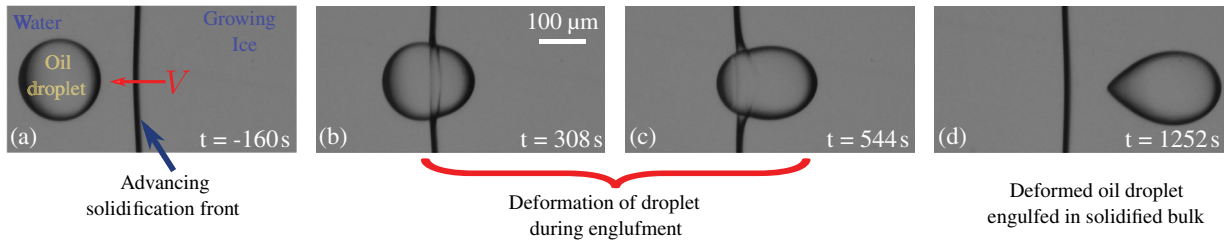

FIG. 2. (a)–(d) Top-view snapshots capturing the engulfment of a 5 cSt silicone oil droplet submerged in water by an advancing solidification front ($V = 0.4 \ \mu m \, s^{-1}$), i.e., ice, first approaching and then passing over the droplet (Supplemental Movie 1). At $t = 0$ the drop makes first contact with the front. The applied temperature gradient G is about 10 K cm^{-1}. The droplet remains deformed in the solidified bulk after engulfment throughout the entire experiment (typically ~ 4 h).
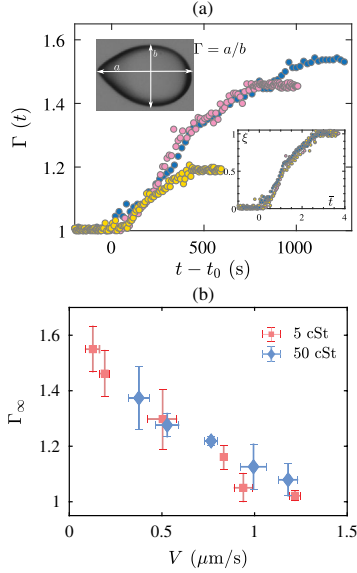
FIG. 3. (a) Aspect ratio $\Gamma(t)$ as a function of time t for advancing velocities $V = (blue\ filled\ circle)\,0.2\ \mu\mathrm{m\,s}^{-1}$ ($pink\ filled\ circle$) $0.4\ \mu\mathrm{m\,s}^{-1}$ ($yellow\ filled\ circle$) $0.6\ \mu\mathrm{m\,s}^{-1}$. The solidification front makes first contact with the droplet at $t = t_0$. The inset shows the universality of the engulfment process, where $\xi = (\Gamma(t) - 1)/(\Gamma_\infty - 1)$ and $\bar{t} = (t - t_0)V/R$. (b) Final aspect ratio Γ_∞ of the deformed droplet in the solidified bulk as a function of the solidification front advancing velocity V for two kinematic viscosities $\nu = (orange\ filled\ square)\,5\ \mathrm{cSt}$ and ($blue\ filled\ diamond$) 50 cSt.

the disjoining pressure length scale, and the exponent η depends on the type of intermolecular forces that dominate; for nonretarded van der Waals interactions, $\eta = 3$ [37]. Note that electrostatic contributions are not taken into account. Crucially, due to the reduction in melting temperature of the bulk in the vicinity of the droplet, a thin liquid film of thickness $H(X)$ persists in the gap between the droplet and the solidifying bulk. Direct imaging of such thin films is challenging because of their small dimensions. However, our experimental setup allows us to observe such thin films as the solidification front passes over the droplet; see Supplemental Material [31]. Here, we hypothesize that it is the spatial pressure variation within this thin film that mediates the overall shape change of the droplet during its engulfment into the solidifying bulk. In the following, we present a model that connects the fluid flow in the enveloping thin film around the droplet to its deformation.

We model the fluid flow in thin intervening liquid films using lubrication theory. The main assumption of our analysis is that the flow during the engulfment process is predominantly in the direction of motion of the solidification front. Accordingly, as illustrated in Fig. 4(b), we treat the intervening thin film as a one-dimensional slab geometry, bounded between the oil-water interface and the growing ice. Fluid motion within the film is mainly driven by a gradient in disjoining pressure due to the variation with film thickness
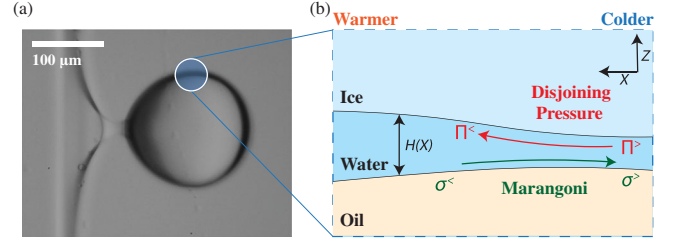

FIG. 4. (a) Experimental image capturing the engulfment of an oil drop (Supplemental Movie 2). (b) The schematics visualizes the competition between the disjoining pressure Π and Marangoni effects that mediate the flow profile within the liquid film with varying $H(X)$. Depending on the profile of the thin film, the pressure in the film p_{film} varies, which determines the local curvature of the oil-water interface and eventually the overall shape of the drop.

($\Pi \sim H^{-3}$) [38], and Marangoni stresses at the droplet interface due to the externally applied thermal gradient G; see the schematic in Fig. 4(b). By making use of the slender geometry of the system, and by applying no-slip and slip boundary conditions at the water-ice and oil-water interfaces as $U|_{(Z=H)} = 0$ and $\mu \partial_Z U|_{Z=0} - \mu' \partial_Z U'|_{Z=0} = \partial_X \sigma$, respectively, where $\partial_Z U' = -\partial_X \sigma/(\mu + \mu')$ [26], the net horizontal flux $q(X)$ is given by

$$\mu q(X) = \frac{1}{2}\frac{d\sigma}{dT}\left[1 - \frac{\mu'}{\mu + \mu'}\right]GH(X)^2 - \frac{1}{3}\partial_X p H(X)^3. \quad (2)$$

Primed quantities refer to the oil phase and unprimed to the water phase. σ is the interfacial tension of the oil-water interface, μ the dynamic viscosity, and $p = -\sigma \partial_X^2 H - A/6\pi H^3$ is the pressure in the thin film in lubrication approximation. Note that the disjoining pressure is also related to the applied thermal gradient as $A/6\pi H^3 = -\rho_s \mathcal{L} GX/T_m$ [34] with A the Hamaker constant. Consequently, the local mass conservation ($\partial_t h + \partial_x q = 0$) in nondimensional form can be expressed as

$$\partial_t h + \partial_x \left[\frac{1}{3Ca}h^3 \partial_x^3 h + \frac{1}{3BrPr}h^3 - \frac{Ma}{Pr}h^2\right] = 0. \quad (3)$$

Note that in the above equation lowercase quantities are nondimensionalized. The droplet radius R is used to nondimensionalize lengths, and the velocity scale is chosen as ν/R. $Ca = \mu\nu/\sigma R$ is the capillary number and $Pr = \nu/\kappa$ the Prandtl number; $\nu = \mu/\rho$ and κ are kinematic viscosity and thermal diffusivity of water, respectively. The other two dimensionless parameters of the problem are the Brinkman number Br and the Marangoni number Ma, defined as

$$Br = \frac{\mu\kappa T_m}{\rho_s \mathcal{L} GR^3}, \qquad Ma = \frac{-(d\sigma/dT)GR^2}{2\mu\kappa}\left[1 - \frac{\mu'}{\mu + \mu'}\right].$$
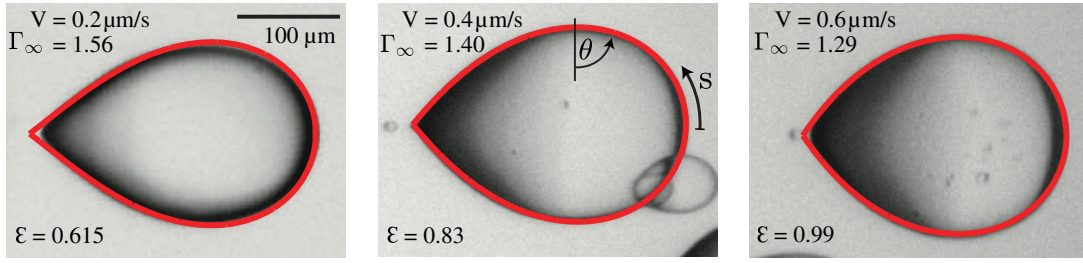$$(4)$$

FIG. 5. Experimental snapshots of three deformed 5 cSt silicone oil droplets that were engulfed at different velocities $V = 0.2\ \mu\text{m s}^{-1}$, $0.4\ \mu\text{m s}^{-1}$, and $0.6\ \mu\text{m s}^{-1}$. The applied temperature gradient G is about $10\ \text{K cm}^{-1}$ and the corresponding final aspect ratios Γ_∞ of their final shapes are also indicated. The lines overlaid in red are the shapes generated by the pendant drop model [39] with corresponding values of the deformation parameter $\mathcal{E}$.

They indicate the strength of the fluid flow driven by intermolecular pressure and of the thermal Marangoni force, respectively. The former expresses the (inverse) ratio of the timescale for diffusive thermal transport ($t_\kappa \sim R^2/\kappa$) to the timescale for convective thermal transport ($t_u \sim \mu T_m / \rho_s \mathcal{L} G R$) that is driven by the gradient in intermolecular pressure. The latter provides an estimate for the (inverse) ratio of the timescale for convective thermal transport ($t_{Ma} \sim -\mu/(d\sigma/dT)G$) driven by the thermal Marangoni force and again the timescale for diffusive transport. Although it is difficult to predict *a priori* whether intermolecular interactions dominate over thermal Marangoni effects or vice versa, by changing the applied thermal gradient G and thus the engulfment velocity $V \propto G$ we can control the relative strength of these two effects and thus the final shape of the droplet.

Since typical timescales associated with the droplet engulfment in our experiments are extremely slow, much larger than the viscous timescale $t_v \sim \mu R/\sigma$, the overall process can be treated as quasisteady. Therefore, the unsteady term $\partial_t h$ in Eq. (3) can be omitted ($\partial_t h = 0$) to determine the steady state of the film thickness as

$$h(x) = \frac{h_0}{R} + \left(\frac{L}{R}\right)^3 \frac{Ca}{6Pr}\zeta(x)\left[\frac{3MaR}{H_0} - \frac{1}{Br}\right]$$
$$+ \frac{1}{2}\frac{p_\infty R}{\sigma}\left[\left(\frac{L}{R}\right)^2 - x^2\right], \quad (5)$$

with $\zeta(x) = [(xR/L)^3 - 3(xR/L)^2 + 2]$. For this result, we have used the boundary conditions $\partial_x^2 h|_{x=L/R} = -p_\infty R/\sigma$, $\partial_x h|_{x=0} = 0$, and $h|_{x=L/R} = H_0/R$, where H_0 is a typical film thickness, L is the length of a stretched droplet, and p_∞ a reference ambient pressure. Notably, this result is in agreement with our experimental observations that, promoted by Marangoni flow, thicker liquid films envelop the droplet at higher engulfment velocities. As the thermal gradient G increases (and thus V) the flow toward the colder side is enhanced, leading to the thickening of the liquid film and hence altering the pressure profile within, causing the drop to deform less, whereas intermolecular

interactions are responsible for its thinning at lower velocities. Further, using the relationship between pressure and film thickness, the lubrication pressure within the thin film is estimated to be

$$\Delta p_{\text{lub}} = \frac{\sigma}{R^2}\frac{Ca}{Pr}\left[\frac{3MaR}{H_0} - \frac{1}{Br}\right](L - X) + \frac{\rho_s \mathcal{L} G}{T_m}X, \quad (6)$$

where $\Delta p_{\text{lub}} = p_{\text{film}} - p_\infty$. It is apparent from the above expression that the lubrication pressure within the intervening thin liquid film, irrespective of the velocity of droplet engulfment, varies linearly along the droplet interface. It also suggests that dynamic Marangoni effects are dominant over intermolecular interactions if $3MaBrR/H_0 < 1$.

To relate the linearly varying pressure in the enveloping thin films with the deformed shape of an engulfed droplet, we use the analogy of a pendant droplet, whose shape is strikingly similar to that of an engulfed droplet. As described in Ref. [39], the canonical interfacial shape of a pendant droplet can be expressed in a nondimensional form as

$$\frac{d^2\theta}{ds^2} = -\sin\theta, \quad (7)$$

where θ is the angle measured through the liquid from the vertical to the tangent, s is the curve-linear coordinate along the interface, and $d\theta/ds$ is the local curvature of the interface. Equation (7) simply represents the balance between surface tension and hydrostatic pressure along the interface of a pendant droplet. Interestingly, the same functional form is also recovered for a droplet enveloped by a thin film in which the pressure varies linearly. We refer to Supplemental Material [31] for a detailed derivation. Accordingly, solving Eq. (7) for given total energy $\mathcal{E} = 1/2(d\theta/ds)^2 - \cos\theta$ yields the deformed shape of the engulfed droplet. This is equivalent to solving a pendulum equation with total energy $\mathcal{E}$, which turns out to be the only parameter of our model. Note that the values of the energy parameter $\mathcal{E}$ are chosen so as to exactly match the aspect ratio of the deformed engulfed droplets. Figure 5 shows an excellent match between the experimentally measured

deformed droplet shapes and our model predictions for $\mathcal{E} = 0.615$, 0.83, and 0.99, respectively.

In summary, in this Letter, we reported that a soft particle when engulfed into a growing crystal sustains mechanical deformations. These deformations are found to strongly depend on the engulfment velocity and to be mediated by pressure variations in the unfrozen thin liquid films intercalating between the particle and the encapsulating crystal. In case of droplets or bubbles, the presence of a free interface evokes thermal Marangoni forces, which critically change the local dynamics. We demonstrated that the strength of the flow driven by Marangoni stresses dictates the thickness of the intervening liquid film, which in turn controls the deformation of the engulfed particle.

Our work quantitatively demonstrates why faster freezing (i.e., larger engulfment velocity V) has a much weaker impact on the soft particle's shape than slow freezing, and what parameters control this process. These findings are extremely relevant for exerting better control over cryo-preservation procedures of food emulsions and biospecimens, where mechanical deformations of the dispersed medium are important to the freeze-thaw stability of the solidified material.

J. G. M. and P. K. contributed equally to this work.

———————

[*]j.g.meijer@utwente.nl
[†]kantpallav88@gmail.com
[‡]d.lohse@utwente.nl

[1] S. Deville, E. Saiz, R. K. Nalla, and A. P. Tomsia, Freezing as a path to build complex composites, Science **311,** 515 (2006).

[2] S. Deville, E. Saiz, and A. P. Tomsia, Ice-templated porous alumina structures, Acta Mater. **55,** 1965 (2007).

[3] S. Deville, Freeze-casting of porous ceramics: A review of current achievements and issues, Adv. Eng. Mater. **10,** 155 (2008).

[4] S. Deville, Freeze-casting of porous biomaterials: Structure, properties and opportunities, Materials **3,** 1913 (2010).

[5] C. Körber, Phenomena at the advancing ice–liquid interface: Solutes, particles and biological cells, Q. Rev. Biophys. **21,** 229 (1988).

[6] K. Muldrew, J. P. Acker, J. A. W. Elliott, and L. E. McGann, *Life in the Frozen State* (CRC Press, Florida, 2004), pp. 93–134.

[7] V. L. Bronstein, Y. A. Itkin, and G. S. Ishkov, Rejection and capture of cells by ice crystals on freezing aqueous solutions, J. Cryst. Growth **52,** 345 (1981).

[8] H. D. Goff, Colloidal aspects of ice creama review, Int. Dairy J. **7,** 363 (1997).

[9] S. Ghosh and J. N. Coupland, Factors affecting the Freeze–Thaw stability of emulsions, Food Hydrocolloids **22,** 105 (2008).

[10] J. F. Crilly, A. B. Russell, A. R. Cox, and D. J. Cebula, Designing multiscale structures for desired properties of ice cream, Ind. Eng. Chem. Res. **47,** 6362 (2008).

[11] S. S. L. Peppin and R. W. Style, The physics of frost heave and ice-lens growth, Vadose Zone J. **12,** 1 (2013).

[12] S. Peppin, A. Majumdar, R. Style, and G. Sander, Frost heave in colloidal soils, SIAM J. Appl. Math. **71,** 1717 (2011).

[13] A. W. Rempel, Frost heave, J. Glaciol. **56,** 1122 (2010).

[14] D. Shangguan, S. Ahuja, and D. M. Stefanescu, An analytical model for the interaction between an insoluble particle and an advancing solid/liquid interface, Metall. Trans. A **23,** 669 (1992).

[15] M. S. Park, A. A. Golovin, and S. H. Davis, The encapsulation of particles and bubbles by an advancing solidification front, J. Fluid Mech. **560,** 415 (2006).

[16] D. Dedovets, C. Monteux, and S. Deville, Five-dimensional imaging of freezing emulsions with solute effects, Science **360,** 303 (2018).

[17] D. R. Uhlmann, B. Chalmers, and K. A. Jackson, Interaction between particles and a solid-liquid interface, J. Appl. Phys. **35,** 2986 (1964).

[18] G. F. Bolling and J. Cisse, A theory for the interaction of particles with a solidifying front, J. Cryst. Growth **10,** 56 (1971).

[19] A. A. Chernov, D. E. Temkin, and A. M. MelNikova, Theory of the capture of solid inclusions during the growth of crystals from the melt, Sov. Phys. Crystallogr. **21,** 369 (1976).

[20] R. R. Gilpin, A model of the "liquid-like" layer between ice and a substrate with applications to wire regelation and particle migration, J. Colloid Interface Sci. **68,** 235 (1979).

[21] R. R. Gilpin, Theoretical studies of particle engulfment, J. Colloid Interface Sci. **74,** 44 (1980).

[22] A. W. Rempel, J. S. Wettlaufer, and M. G. Worster, Interfacial Premelting and the Thermomolecular Force: Thermodynamic Buoyancy, Phys. Rev. Lett. **87,** 088501 (2001).

[23] A. W. Rempel, J. S. Wettlaufer, and M. G. Worster, Premelting dynamics in a continuum model of frost heave, J. Fluid Mech. **498,** 227 (2004).

[24] A. W. Rempel and M. G. Worster, The interaction between a particle and an advancing solidification front, J. Cryst. Growth **205,** 427 (1999).

[25] J. N. Israelachvili, *Intermolecular and Surface Forces* (Academic Press, New York, 2011).

[26] N. O. Young, J. S. Goldstein, and M. J. Block, The motion of bubbles in a vertical temperature gradient, J. Fluid Mech. **6,** 350 (1959).

[27] Y. E. Geguzinand A. S. Dzuba, Crystallization of a gas-saturated melt, J. Cryst. Growth **52,** 337 (1981).

[28] B. Van Elburg, G. Collado-Lara, G.-W. Bruggert, T. Segers, M. Versluis, and G. Lajoinie, Feedback-controlled microbubble generator producing one million monodisperse bubbles per second, Rev. Sci. Instrum. **92,** 035110 (2021).

[29] J. C. T. Kao, A. A. Golovin, and S. H. Davis, Particle capture in binary solidification, J. Fluid Mech. **625,** 299 (2009).

[30] S. Tyagi, C. Monteux, and S. Deville, Solute effects on the dynamics and deformation of emulsion droplets during freezing, Soft Matter **18,** 4178 (2022).

[31] See Supplemental Material at http://link.aps.org/supplemental/10.1103/PhysRevLett.130.214002 for a broader discussion on the general experimental details and a more detailed derivation of Eq. (7).

[32] J. G. Dash, H. Fu, and J. S. Wettlaufer, The premelting of ice and its environmental consequences, Rep. Prog. Phys. **58,** 115 (1995).

[33] J. G. Dash, A. W. Rempel, and J. S. Wettlaufer, The physics of premelted ice and its geophysical consequences, Rev. Mod. Phys. **78,** 695 (2006).

[34] J. S. Wettlaufer and M. G. Worster, Premelting dynamics, Annu. Rev. Fluid Mech. **38,** 427 (2006).

[35] M. Perez, Gibbs–thomson effects in phase transformations, Scr. Mater. **52,** 709 (2005).

[36] B. V. Derjaguin, Definition of the concept of and magnitude of the disjoining pressure and its role in the statics and kinetics of thin layers of liquid, Colloid J. USSR **17,** 191 (1955).

[37] J. S. Wettlaufer, M. G. Worster, L. A. Wilen, and J. G. Dash, A Theory of Premelting Dynamics for All Power Law Forces, Phys. Rev. Lett. **76,** 3602 (1996).

[38] B. Dai, L. G. Leal, and A. Redondo, Disjoining pressure for nonuniform thin films, Phys. Rev. E **78,** 061602 (2008).

[39] B. Roman, C. Gay, and C. Clanet, Pendulums, drops and rods: A physical analogy, arXiv:2006.02742.